OVERCOMING OBSTACLES IN DISPERSION MODELING AT DIABLO CANYON NUCLEAR POWER PLANT

by

Richard H. Thuillier
Pacific Gas and Electric Company
2303 Camino Ramon, Suite 200
San Ramon, CA 94583

April, 1996

INTRODUCTION

Historically, there have been several challenges to simulating transport and dispersion of effluent releases at Diablo Canyon Nuclear Power Plant (DCPP): locating representative measurement sites to represent meteorological conditions at the site of release; representing the dispersive effect of complex plant structures, and representing the effect of the surrounding complex terrain on transport and dispersion (Figure 1). Since temporal meteorological variability is also a factor, forecasting (projecting) plume transport trajectories is also a challenge. Sulfurhexafluoride gas tracer experiments conducted in 1976 identified a variety of transport trajectories and their temporal variability for effluent released at the plant (Figure 4a). Simulation of variable trajectories was addressed by modeled transport of Gaussian puffs through a diagnostic wind field based on measurements throughout the surrounding terrain. The model (PGEMS) was developed under contract to PG&E by Battelle, PNL (Allwine, 1993). Initial comparison of model estimates with measured tracer concentrations revealed a substantial model overestimate of measured concentrations, both in the near field (12 building heights downwind) and in the far field (10 kilometers or more downwind). The near-field problem was addressed successfully by incorporating a recently developed wake algorithm into the Gaussian puff model (Ramsdell, 1990). The far-field problem has been addressed by accepting Gaussian estimates as inherently conservative in the far field due to an unsimulated, terrain induced, enhanced dispersion . Forecasting complex transport patterns has been addressed by using historical data to produce the hourly probability of occurrence of representative wind flow patterns defined by network measurements. While these approaches are not currently incorporated in official procedures for emergency response at DCPP, they are available for use by PG&E meteorologists, on a consultation basis, to guide emergency response decisions.

STRUCTURAL WAKE EFFECTS

Formulation of Algorithms

Wake correction algorithms for Gaussian models have been formulated over the years to address enhanced dispersion due to structure-induced turbulence near the source. Based on theory, observation, and wind tunnel modeling, these algorithms have for the most part simply enhanced the Gaussian sigma values near the source in relation to the dimensions of the turbulence-inducing structures. One of the earliest models, underlying past wake correction recommendations by the Nuclear Regulatory Commission (NRC), is that attributed to Fuquay by Gifford (1960) in the form

$$X = Q/[\pi U(\sigma_y\sigma_z+cA/\pi)] \qquad (1)$$

where **X** is concentration, **Q** is emission rate, **U** is the mean wind speed at release, σ_y and σ_z are the statistical parameters of horizontal and vertical plume spread, **A** is the cross-sectional area of the wake-inducing structures, and **c** is a constant valued between 0.5 and 1.5.

In equation (1), the product $\sigma_y\sigma_z$ has been enhanced by a constant multiple $\mathbf{c/\pi}$ of the structure vertical cross sectional area **A**. A more recent example of such modeling is the wind tunnel-based Huber-Snyder algorithm (Huber et al., 1982) which is the basis for wake adjustment in the Indirect Source Complex (ISC) model recommended by the U.S. Environmental Protection Agency (EPA). In the EPA model (Trinity Consultants, 1992), the Gaussian sigmas are individually enhanced as functions of the horizontal and vertical dimensions of the wake inducing structures and downwind travel distance.

Data from gas tracer experiments at a number of nuclear power plants [Thuillier (1982), Ramsdell (1990)] have revealed several characteristics of wake-induced dispersion not well represented by such models. One of these is the tendency for wake-affected ground-level concentration to decrease significantly and systematically as wind speed decreases; a second is the tendency for wake effects to persist at downwind distances exceeding the assumptions of the wake models; and a third is the tendency for complex structures to produce plume centerline downwash as well as enhanced dispersion for roof-top releases.

Based on empirical and theoretical considerations, Ramsdell (1990) proposed a time-based wake algorithm for ground-level releases that appeared to provide a greatly improved treatment of wake-affected dispersion. The 1990 Ramsdell algorithm defined Gaussian variance in a structural wake, $(\Delta\sigma)_w^2$, as a function of the Lagrangian autocorrelation function for background turbulence, **r**, a wake-induced increment in the lateral component of upwind turbulence, $(\Delta\sigma)^2$, and a time scale for turbulent decay, **T**, in the general form:

$$(\Delta\sigma_{y,z})_w^2 = [KT^2][1-(1+t/T)\exp(-t/T)] \qquad (2)$$

where $\mathbf{K = 2r(\Delta\sigma)^2}$ has an assumed default value of 1 and is suggested as a model calibration factor. The term $\mathbf{KT^2}$ determines the maximum increment to the diffusion component and the right bracketed term determines the fraction applied as travel time increases.

Horizontal ($\mathbf{T_h}$) and vertical ($\mathbf{T_v}$) time scales were defined by Ramsdell as

$$\mathbf{T_h = A^{1/2}/u^*} \qquad (3)$$

$$\mathbf{T_v = T_h/(2+z/L)} \qquad (4)$$

where

u^* = friction velocity
L = Monin-Obukhov length, and
z = height above ground (assumed as 10 m)

These wake induced variance enhancements were then combined with the variances associated with ambient turbulence $(\sigma_{y,z})_a^2$ as a root sum of squares to produce total sigmas in the form:

$$\Sigma_y = [(\Delta\sigma_y)_w^2 + (\sigma_y)_a^2]^{1/2} \quad (5)$$

$$\Sigma_z = [(\Delta\sigma_z)_w^2 + (\sigma_z)_a^2]^{1/2} \quad (6)$$

These total sigmas can then be used in the standard Gaussian plume equations.

Based on peer review (Briggs et al., 1992; Ramsdell and Fosmire, 1995), the algorithm for wake-induced dispersion was reformulated by restricting the wake induced $(\Delta\sigma)_w^2$ variance component to higher wind speeds and introducing a separate non-wake $(\Delta\sigma)_{lw}^2$ variance component to account for meander assumed responsible for concentration decrease at low wind speeds. All variance components have the same equation (2) formulation and the total variance now has the three-component form:

$$\Sigma_y = [(\Delta\sigma_y)_{lw}^2 + (\Delta\sigma_y)_w^2 + (\sigma_y)_a^2]^{1/2} \quad (7)$$

$$\Sigma_z = [(\Delta\sigma_z)_{lw}^2 + (\Delta\sigma_z)_w^2 + (\sigma_z)_a^2]^{1/2} \quad (8)$$

Based on the literature and peer review suggestions, the $2R(\Delta\sigma)^2$ portion of equation (2) was redefined as

$$\mathbf{[2(0.655)(0.835)^2]\ and\ [2(0.584)(0.239)^2]} \quad (9)$$

respectively, for the horizontal and vertical components of the low wind speed variance and as

$$\mathbf{[2(0.655)(0.02U^2)^2]\ and\ [2(0.584)(0.01U^2)^2]} \quad (10)$$

respectively, for the horizontal and vertical components of the wake-induced variance.

Based again on literature, the time scales for low wind speed and wake conditions were redefined as

$$\mathbf{(T_h)_{lw} = 1000\ sec;} \quad (11)$$

$$\mathbf{(T_v)_{lw} = 100\ sec;} \quad (12)$$

$$\mathbf{(T_h)_w = (T_v)_w = 10(A)^{1/2}/U} \quad (13)$$

Evaluation at DCPP

Figures 2 and 3 provide a comparison of prediction by the various wake algorithms as a function of wind speed and downwind distance, respectively. Tracer data from a ground level release at the base of the Unit 2 containment building (Figure 1) is provided for a downwind distance of approximately 12 building heights (840 m) downwind. Data are maximum hour-averaged tracer concentrations measured on a sampling arc (assumed to approximate plume centerline concentrations). Data were carefully chosen to represent uniform meteorological conditions without significant ambient meander, consisting of D stability, based on 15-minute measurements of sigma-theta, and hourly ranges of 5-minute averaged wind direction less than 16 degrees. Except for the Ramsdell models, which are formulated only for a ground-level release, wake models typically assume, in the case of elevated releases, that plume centerlines remain at the height of release plus plume rise. A tendency for possible plume centerline downwash as reported by Thuillier (1982) is conservatively handled in the puff modeling by assuming that all releases are at ground level.

Figure 2 provides a striking illustration of the relationship of wake-affected ground-level concentration to wind speed. The relative skill of the various wake algorithms in dealing with the characteristics of wake-affected concentration is evident from the figure. Lack of meander in the ambient wind data associated with the plotted tracer measurements suggests that the enhanced dispersion at low wind speeds might be structurally (though not necessarily aerodynamically) induced and not simply an artifact of ambient meander. Figure 3 illustrates the ability of the Ramsdell algorithms to reflect a greater downwind persistence of wake-induced dispersion enhancement.

TERRAIN EFFECTS

Definition of Wind Patterns

Figure 4a, based on the 1986 tracer data, illustrates the variability of transport trajectories in the vicinity of DCPP and the location of six critical wind measurement sites that provide information on associated wind flow patterns. These trajectories represent paths of plant effluent transport through terrain-induced patterns of wind flow that change hour-by-hour and day-by-day. In the event of a radiological release, the ability to identify and forecast the wind patterns responsible for the transport trajectories is important imput to protective action recommendations in the various protective action zones surrounding the plant (Figure 1). In an effort to characterize these wind flow patterns in some straightforward manner, an analysis was done of a data set representing each hour of each day of the year (by merging two years of partial data), obtained from the six critical sites (Thuillier, 1989). The study indicated that if four directional quadrants were established, representing wind flow along or across the natural orientation of the terrain (Figures 1 and 4a), 10-m quadrantal wind directions measured at three-station subsets of the six measurement sites could be used to define a concise set of 12 surface wind direction patterns. These patterns adequately represent significant possibilities for terrain-influenced transport in the vicinity of DCPP relative to the spatially extensive protective action zones.

Figure 4b defines the 12 patterns in terms of quadrantal wind directions at the measurement sites. Each pattern (Figure 5) is defined in terms of three characteristics: a primary characteristic of initial transport, based on wind direction at DCPP (the plant primary tower site), a secondary characteristic of downwind inland valley penetration, based on quadrantal wind direction at valley entry/exit sites CEM or VCNTR, and a tertiary characteristic of the direction and extent of inland valley penetration when it occurs, based on quadrantal wind direction at the more inland sites DVPK, FTHILL, or SVCNTR.

The three characteristics are given a letter/number/letter code to identify the pattern. Thus pattern NW2B represents an initial flow toward the SE due to NW winds at DCPP, inland penetration due to southerly sea breeze winds at site VCNTR, and deep penetration based on observed southerly winds, also at site SVCNTR.

The wind pattern classification scheme just described serves several useful purposes:

- Measured winds at the six sites can be used to produce diagnostic modeled wind fields corresponding to the 12 basic patterns.
- Databases can be readily searched to produce statistics on the annual, seasonal, and diurnal occurrence of wind patterns.
- Wind pattern statistics can be used to provide probabilistic forecasts of wind pattern evolution.

Speed statistics for the wind patterns are also available as in Table 1.

Wind Pattern Forecasting at DCPP

Based on the "full year" of wind data described above, a useful computer program has been developed (Holets and Thuillier, 1991) for wind pattern forecasting at DCPP. Given an input set of initial conditions at the time of forecast, the program searches available historical data and outputs the expected frequency of occurrence of each wind pattern for the next 24 individual hours (Table 2). The occurrence frequencies shown in Table 2 reflect a pattern of clockwise rotation common to winds in the area, from SE (at initial time of 6 a.m.) through SW through NW as the sea breeze develops.

The most basic input to the forecast model is simply 10-m wind speed and direction at each of the six network sites for the time of forecast. Beyond that, the user can specify, if desired, characteristics of stability, inversion structure, and/or upper air wind flow. Ranges of input values can also be specified to produce a larger sample, to reflect uncertainty in initial conditions, or to focus on a specific season.

Local Wind Variability

The Nuclear Regulatory Commission requires both a primary and a back-up tower at nuclear plant sites. At DCPP, these towers are separated by 1.2 km. Each tower has two levels of measurement. The primary tower provides wind measurements at 25 ft and 76 m, while the back-up tower has wind measurement levels at 10 m and 60 m. A Doppler acoustic sounder with 30-m range gates is also available at the backup tower site. These multi-level dual location sites provide an opportunity to evaluate terrain-induced horizontal and vertical variability in the local wind.

Table 3 illustrates the joint frequency of wind patterns and Doppler-measured upper-level wind directions, while Table 4 illustrates the joint frequency of quadrantal wind direction at different tower locations and levels. This local variability in wind direction, sometimes quite significant, would introduce uncertainty to any modeling based on a single on-site measurement.

SUMMARY

A wake-adjusted, diagnostic wind field driven Gaussian puff model has been developed by PG&E to address transport and dispersion influence of plant structures and complex terrain at the Diablo Canyon Nuclear Power Plant. A statistical scheme has been developed for forecasting representative wind patterns based on measurements from a supplemental meteorological measurement network surrounding the plant. With these data and modeling tools, PG&E meteorologists stationed at the DCPP Emergency Operations Facility during emergency situations can offer affective guidance for protective action.

REFERENCES

Allwine, K.J., 1993. *PGEMS - an atmospheric dispersion model for emergency response.* Proc. American Nuclear Society Topical Meeting on Environmental Transport and Dosimetry. Charleston SC.

Briggs, G.A., A.H. Huber, W.H. Snyder and R.S.Thompson, 1992. *Discussion on Diffusion in building wakes for ground-level releases.* Atmospheric Environment 26B, 513-517.

Gifford, F.A., 1960. *Atmospheric dispersion calculations using the generalized Gaussian plume model.* Nucl. Saf.2, 56-59.

Huber, A.H. and Snyder, W.H., 1982. *Wind tunnel investigation of the effects of a rectangular building on dispersion of effluents from short adjacent stacks.* Atmospheric Environment 16, 2837-2848.

Ramsdell, J.V., Jr., 1990. *Diffusion in building wakes for ground-level releases.* Atmospheric Environment 24B, 377-388.

Ramsdell, J.V., Jr. and Fosmire, C.J., 1995. *Atmospheric dispersion estimates in the vicinity of buildings*. Report No. PNL-10286, Pacific Northwest Laboratory, Richland, WA.

Thuillier, R.H., 1982. *Dispersion characteristics in the lee of complex structures*. J. Air Pollut. Cont. Assoc. 32, 526-532.

Thuillier, R.H., 1989. *Wind patterns and their frequency of occurrence in the vicinity of the Diablo Canyon Nuclear Power Plant*. Unnumbered report of Pacific Gas and Electric Company, Meteorologiy Services.

Trinity Consultants, 1992. *EPA users guide for the industrial source complex (ISC2) dispersion models, Volume II - Description of model algorithms*. Dallas, TX.

Table 1. Relative Occurrence Frequency (%) of Speed Ranges Corresponding to Representative Wind Direction Patterns.

Directional	Nighttime Speed Ranges (mph)				Daytime Speed Ranges (mph)			
Wind Patterns	0-3	4-10	11-20	>20	0-3	4-10	11-20	>20
NE1	45	48	7	0	6	81	12	0
NE2	27	65	7	0	0	67	33	0
SE1	45	48	7	*	8	62	30	0
SE2A	33	65	2	0	5	85	9	0
SE2B	48	51	1	0	14	83	2	2
SE2C	67	29	4	0	9	82	9	0
SW1	43	46	11	0	41	46	6	8
SW2A	50	46	4	0	41	57	3	0
SW2B	29	51	17	0	9	45	14	32
NW1	14	51	32	2	2	20	38	41
NW2A	29	63	7	3	8	60	31	2
NW2B	9	59	31	0	1	16	55	28
ALL	31	51	16	0	6	34	32	28

* = < 0.5%

Table 2. Illustration of a Probabilistic Wind Pattern Forecast Made at 6:00 A.M. PST on December 12, 1995 With Initial Wind Pattern SE1

Time (PDT)	Hours After Fcst.	Number of Previous Subsequent Occurrences*											
		NE1	NE2	SE1	SE2A	SE2B	SE2C	SW1	SW2A	SW2B	NW1	NW2A	NW2B
		1	2	3	4	5	6	7	8	9	10	11	12
7	1			21				6					
8	2	6		19							6		
9	3			19									
10	4			12	10						8		
11	5				10						6		
12	6				6	7						7	
13	7								8		9	6	
14	8										13	6	
15	9										16		
16	10										20		
17	11										22		
18	12										21		
19	13										22		
20	14										22	6	
21	15										21		
22	16										22		
23	17										20		
24	18			6							17		
1	19										15		
2	20			8							13		
3	21			14							13		
4	22			10							11		
5	23			10							13		
6	24			10							12		

* Only 5 or more subsequent occurrences are shown

Table 3. Joint Relative Frequency (%) of Surface Directional Wind Patterns and Upper Air Doppler Winds at DCPP

Directional* Pattern	Directional Quadrant* at 190 m AGL					Directional Quadrant* at 310 m AGL				
	NE	SE	SW	NW	Cases	NE	SE	SW	NW	Cases
NE1	38	28	6	27	285	49	16	3	31	87
NE2	40	12	1	47	164	51	11	2	37	65
SE1	15	63	5	17	629	36	37	7	20	162
SE2A	8	71	10	11	89	10	71	5	14	42
SE2B	9	63	16	12	32	22	33	0	24	9
SE2C	21	41	6	32	146	45	23	8	23	64
SW1	30	28	8	35	115	53	25	0	22	59
SW2A	1	49	31	18	71	18	50	11	21	28
SW2B	3	16	3	78	37	0	0	0	100	11
NW1	9	7	3	81	359	13	6	3	70	181
NW2A	6	12	12	70	220	15	28	15	42	97
NW2B	3	9	2	86	1374	7	12	7	57	553
ALL	14	24	5	56	3660	27	18	5	49	1417

Note: Due to rounding and missing data, frequencies do not always add up to 100 %.

Table 4. Relative Joint Occurrence (%) of Quadrantal Wind Direction at Various DCPP Tower Level;

Direction* at Primary Tower 10 m level	Joint Occurrence Frequency of DCPP Direction at Other Tower Levels			
	Primary Tower 76 m level	Backup Tower 10 m level	Backup Tower 60 m level	Both Towers All levels
NE	65	72	65	42
SE	81	75	81	63
SW	51	48	51	26
NW	90	88	90	81

*** direction wind is from**

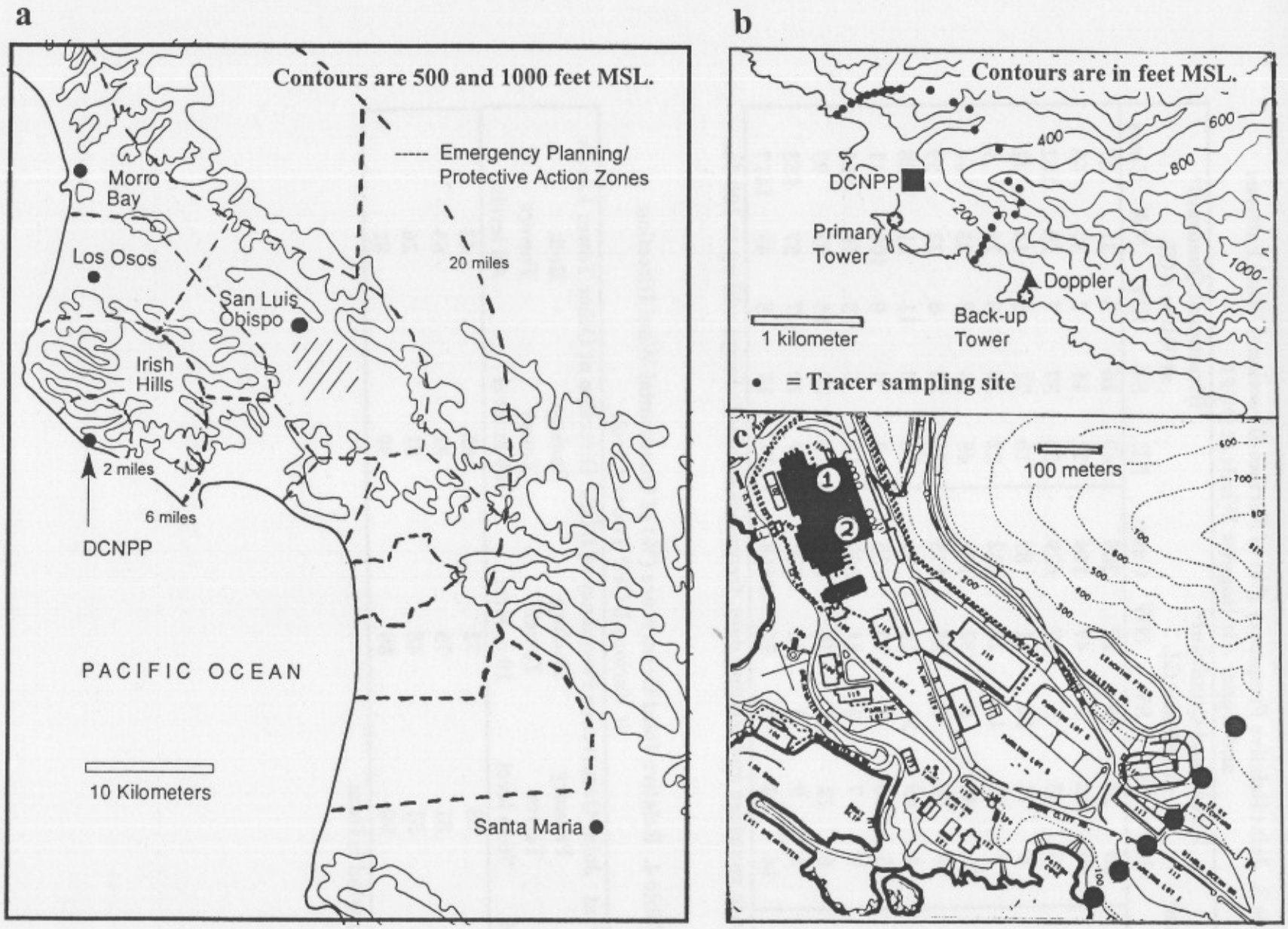

Figure 1. Terrain, plant structures, tracer sampling sites, meteorological towers, and emergency planning/protective action zones in the vicinity of Diablo Canyon Nuclear Power Plant.

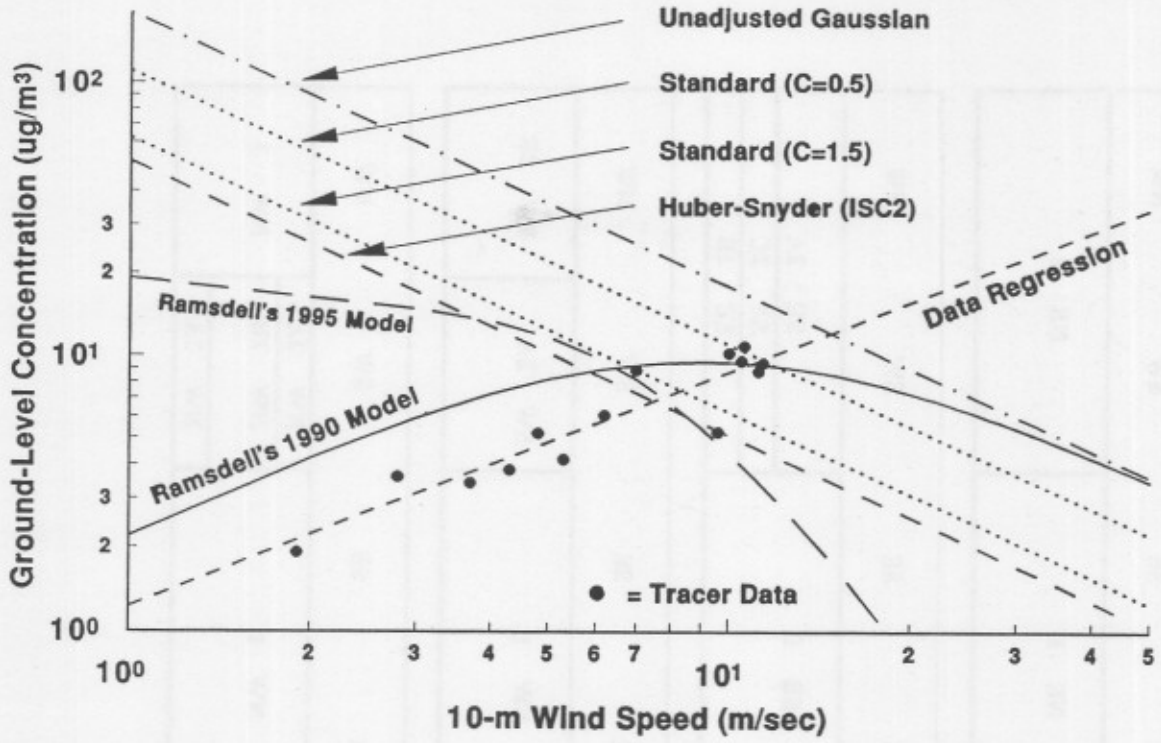

Figure 2. Comparison of DCPP tracer data with wake model estimates (concentration versus 10-m wind speed for D stability at 12 building heights downwind)

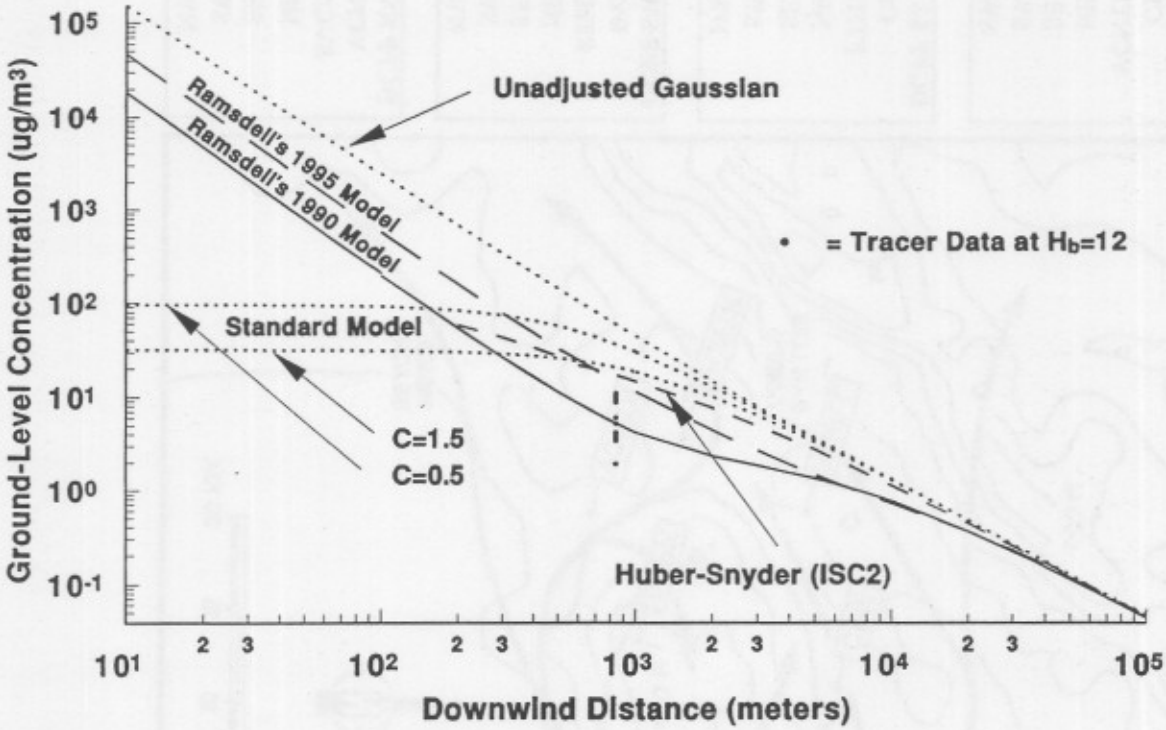

Figure 3. Comparison of DCPP tracer data with wake model estimates (concentration versus downwind distance for D stability)

a

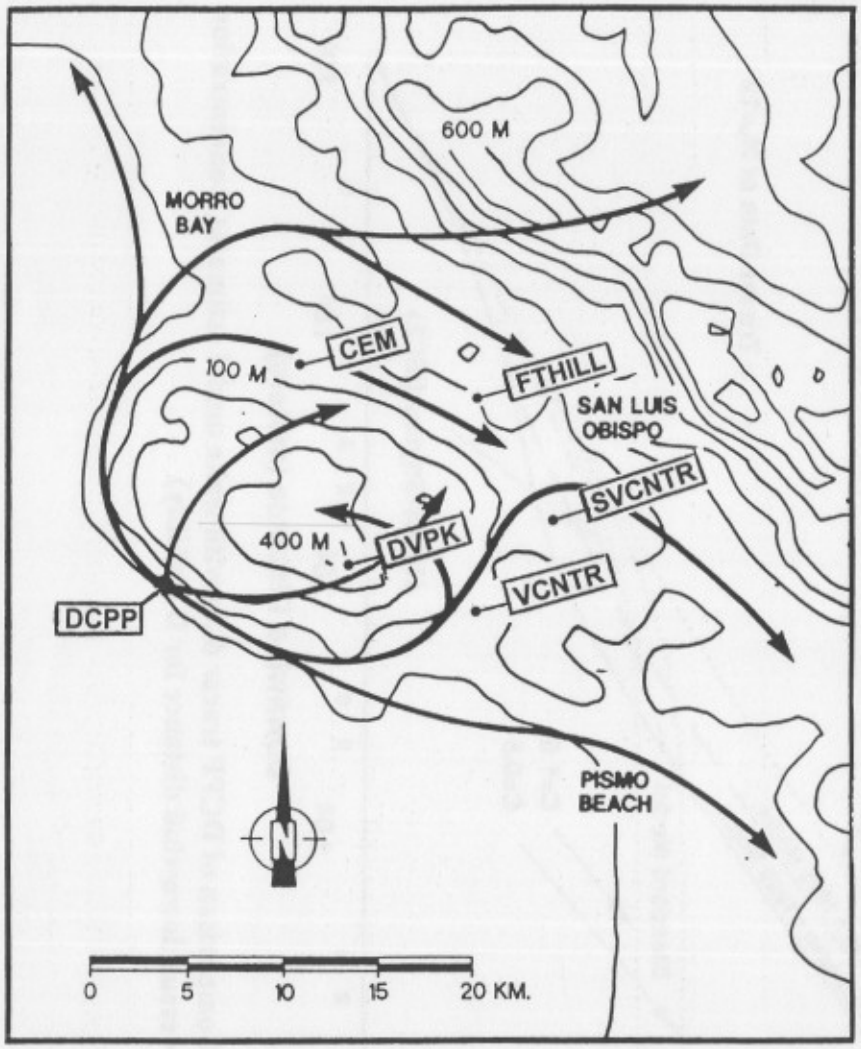

b

DCPP NE CEM> VCNTER	NE	SE	SW	NW
NE	NE 1		NE 2	
SE				
SW				
NW				

DCPP SE CEM> FTHILL	NE	SE	SW	NW
NE	SE 1		SE 2A	
SE				
SW			SE 2C	
NW			SE 2B	

DCPP SW DVPK> FTHILL	NE	SE	SW	NW
NE	SW 1		SW 2A	SW 2B
SE				
SW				
NW				

DCPP NW VCNTR> SVCNTR	NE	SE	SW	NW
NE	NW 1		NW 2A	NW 1
SE			NW 2B	
SW				
NW			NW 2A	

Figure 4. Terrain induced effluent trajectories and wind pattern definitions.

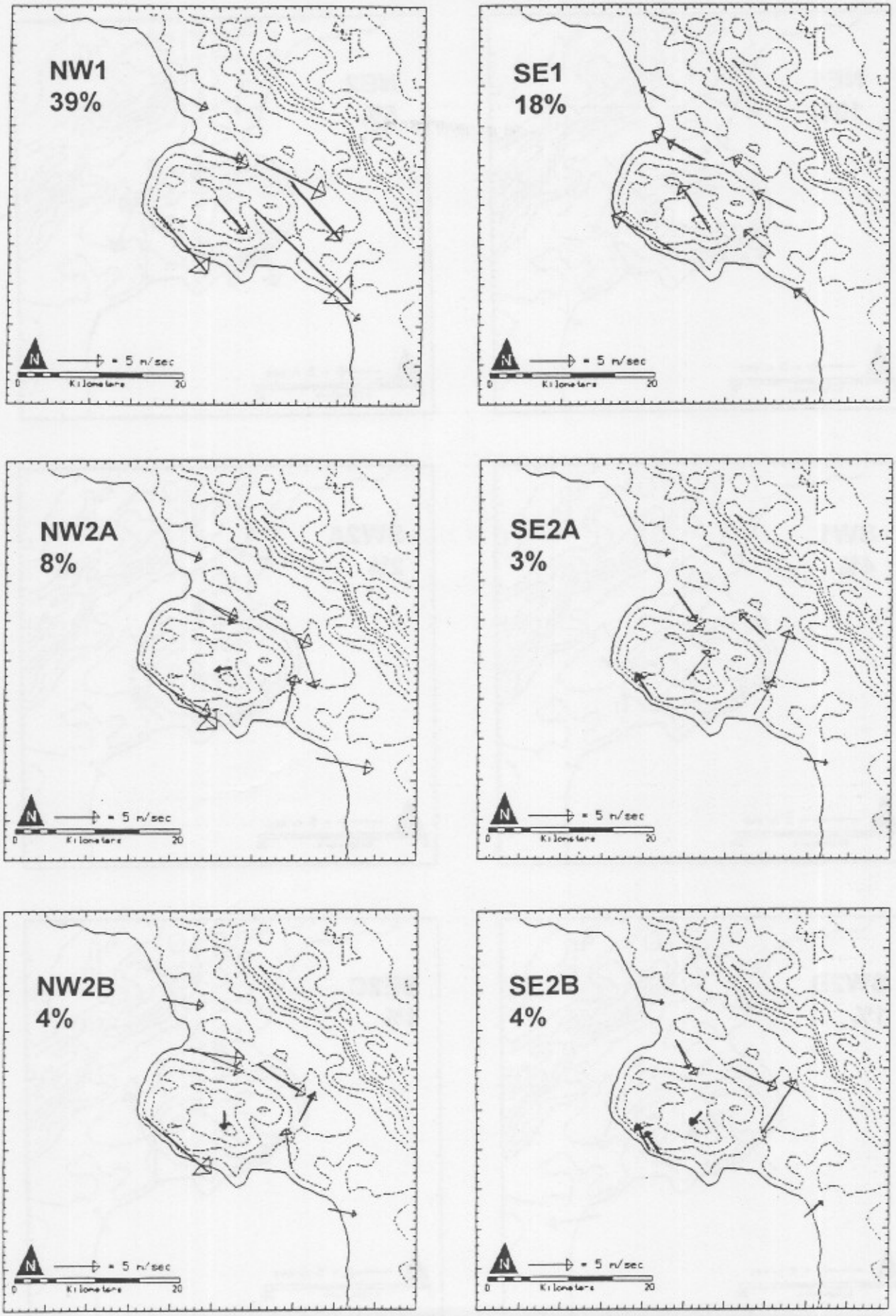

Figure 5. Representative wind patterns and their annual relative frequency for the vicinity of Diablo Canyon Nuclear Power Plant.

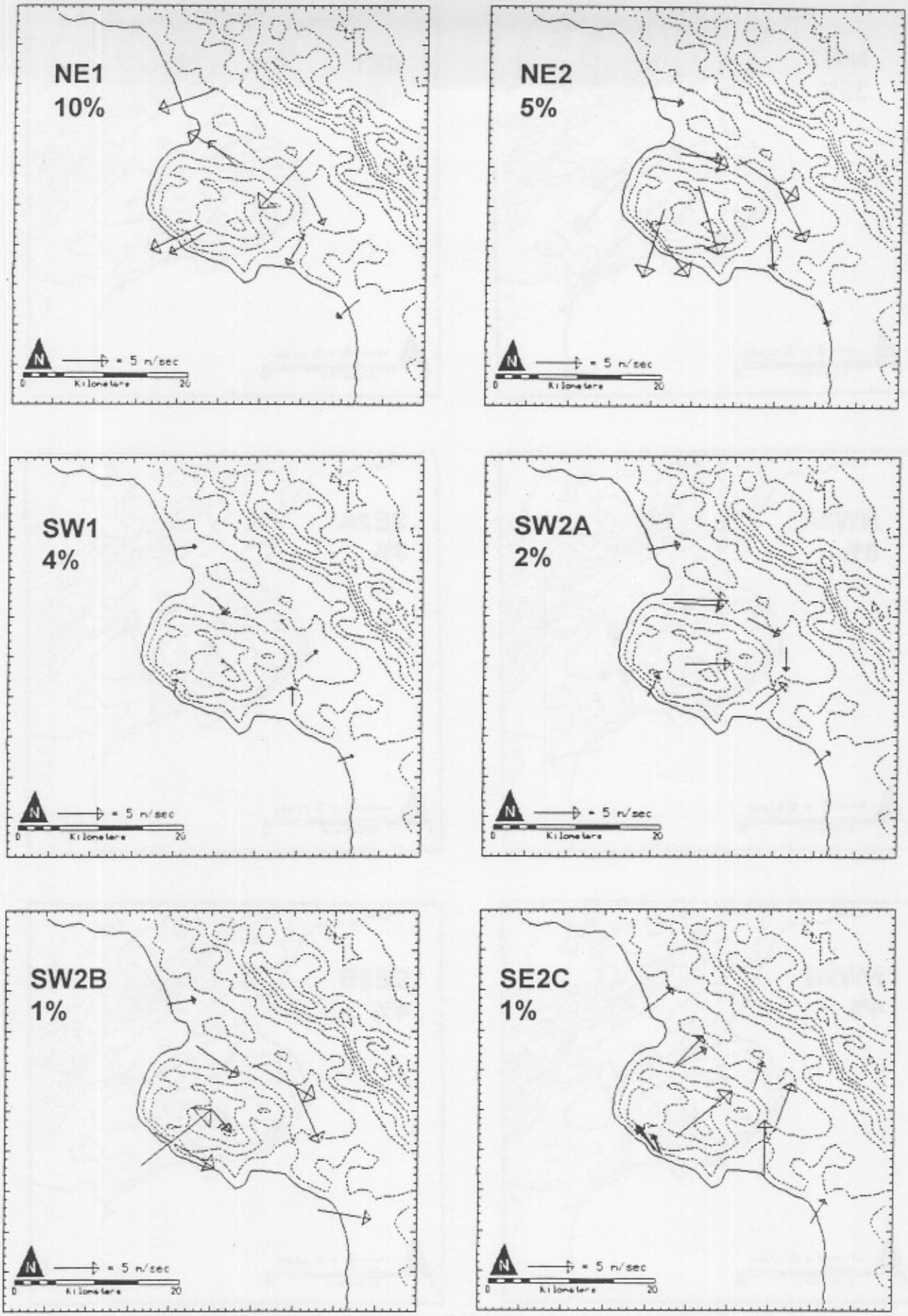

Figure 5. (continued). Representative wind patterns and their annual relative frequency for the vicinity of Diablo Canyon Nuclear Power Plant.